metals

MDPI

Article

The Evolution of Microstructures and the Properties of Bulk Metallic Glass with Consubstantial Composition Laser Welding

Pingjun Tao *, Wenwu Zhang, Qi Tu and Yuanzheng Yang

School of Materials and Energy, Guangdong University of Technology, Guangzhou 510006, China; but98@126.com (W.Z.); nanomatergdut@163.com (Q.T.); taoran200199@163.com (Y.Y.)

* Correspondence: pjtao@gdut.edu.cn; Tel./Fax: +86-20-3932-2570

Academic Editor: Hugo F. Lopez

Received: 20 July 2016; Accepted: 13 September 2016; Published: 29 September 2016

Abstract: A $Zr_{55}Cu_{30}Ni_5Al_{10}$ plate-like bulk metallic glass (BMG) was prepared using copper mold suction casting. Additionally, alloy powders with the same nominal composition were synthesized. The alloy powders were welded or melted to the cleaned surface of the BMG with a laser beam acceleration voltage of 60 kV, a beam current range from 60 to 100 mA, a welding speed of 60 mm/s, as well as an impulse width of 3.0 ms. The effect of consubstantial composition welding on the microstructures and properties was investigated. The molten and subsequently solidified metallic mixtures remain an amorphous structure, but the enthalpy of the welded or melted position varies due to the combination of the micro-structural relaxation and nano-crystals precipitated during the energy inputs. The surface layers of the BMG can be significantly intensified after welding processes; however, the heat-affected zones (HAZs) exhibit a slight degradation in mechanical properties with respect to the BMG matrix. This study has important reference value for specialists working on the promotion of applications of BMGs.

Keywords: bulk metallic glass; consubstantial composition welding; coating; heat affected zones; hardness

1. Introduction

Microstructures of the surfaces and interfaces in materials are important factors to determine their performances [1,2]. Due to their unique structures and properties, amorphous materials have attracted the extensive attention of researchers [3–5]. At present, with science and technology changing with each passing day, the new material industries have been greatly developed. New materials, including amorphous materials [6], are gradually moving from the laboratory to engineering applications, promoting the continuous progress of human societies. It is well known that metallic glasses, including bulk metallic glasses (BMGs), are ideal model systems of dense random packing [7,8]. Compared to crystalline materials, BMGs have a homogenous composition structure, i.e., an isotropy structure. Due to their special matrix structure, BMGs possess many excellent properties that crystalline materials lack and that can serve as potential structural and functional materials in the future in engineering applications, sports equipment, scientific research, and so on [9,10]. BMGs have been found in many different alloy groups, such as Pd-, Mg-, Ln-, Ti-, Fe-, Co-, Ni-, Ca-, Zr-, and Cu-based systems [3], and new alloys have been fabricated and reported with a variety of different properties. Nowadays, a substantial amount of research has been carried out and is being carried out on BMGs investigating their structural and thermal stabilities, mechanical properties, fracturing behavior, preparation and glass-forming abilities, and so on [11,12]; meanwhile, impurity diffusions in the amorphous alloys have been studied primarily [13–15]. However, in BMGs, the welding performance research, which

is an important field that should be carried out and has close relations to mechanical properties and structural and thermal stabilities, have rarely been reported. The importance of weldability in BMGs can be externalized in two aspects as described below. (1) In practical applications, the structural or functional materials with complex external shapes are being widely exploited. However, most reports in academic literature for BMGs only focus on simple shapes, achievable with simple molds [16–18]. The glass forming abilities (GFAs) and preparation methods have confined the synthesis of complex BMG parts. Eventually, the simple shapes, such as those that are rod-like, plate-like, and tube-like shapes, significantly limited the applications of BMGs, wherein welding is the simplest and most effective approach to settle the above-mentioned problems. (2) Papers on welding performances in BMGs are very few [19–21]. Whether welding would affect or modify the BMG matrix structures, or the thermal stabilities and properties, is not clear. Therefore, the weldability research for BMGs is of great significance.

Nowadays, the welding research on BMGs is mostly concentrated on dissimilar welding between BMGs and other alloys, and the contents are only limited to whether the welding is a success [20–22]. However, consubstantial welding research on amorphous alloys using lasers has never been reported. In order to solve partial welding problems, we simplify the welding objects, of which one is the BMG matrix and the other is the consubstantial powder. In the present paper, BMG with a nominal composition of $Zr_{55}Al_{10}Ni_5Cu_{30}$ was selected due to its high GFA [18]. The alloy powders were welded or melted to the cleaned surface of a BMG plate (corresponding to the first aspect (1)) with a laser beam acceleration voltage of 60 kV, a beam current range from 60 to 100 mA, a welding speed of 60 mm/s, as well as an impulse width of 3.0 ms. The effect of consubstantial composition welding on the microstructures and properties of BMG (corresponding to the second aspect (2)) was then investigated. The molten and subsequently solidified metallic mixtures (welds) remain an amorphous structure, but the enthalpy of the welded or melted position varies due to the combination of the micro-structural relaxation and nano-crystals precipitated during the energy inputs. The surface layers of the BMG can be significantly intensified after welding processes; however, the heat-affected zones (HAZs, the area of the BMG matrix near the weld, which is not melted and has had its microstructure and properties altered by laser welding) exhibit a slight degradation in mechanical properties with respect to the BMG matrix. This study has an important reference value for specialists working on the promotion of applications of BMGs.

2. Experimental Procedures

Plate-like $Zr_{55}Cu_{30}Ni_5Al_{10}$ BMG was prepared using copper mold suction casting. Additionally, alloy powders with the same nominal composition were synthesized by intermixing pure Zr, Cu, Ni, and Al powders through ball milling for 24 h. Then, the alloy powders were welded or melted to the cleaned surface of the BMG with a laser beam acceleration voltage of 60 kV, a beam current range from 60 to 100 mA, a welding speed of 60 mm/s, as well as an impulse width of 3.0 ms. After welding, the superfluous alloy powders and semicircle mulches in the surface of the BMG plate were removed, respectively. Then, the BMG plate was ground and polished close to its original state. The structures of the as-cast alloy plate and the alloy powders as well as the removed mulches corresponding to the welds were characterized by using an XD-2 X-ray diffractometer with Cu$K\alpha$ radiation. The thermal properties of the BMG matrix and the removed mulches corresponding to the welds were examined by using an XDT2960 differential scanning calorimeter at a heating rate of 20 K/min in a flow of purified nitrogen gas. The precipitated crystallites were observed by using a high-resolution TEM operated at 200 kV. TEM specimens were prepared by an ion milling with 3 kV and an angle of 4~5 degree mechanical grinding. Surface micro-hardness of the BMG matrix and welds was measured on a Mitutoyo MVK-H3 Hardness Testing Machine. The load was elected as 2N with a dwell time of 10 s. The hardness values in the present paper were the average of six measured points, respectively.

3. Results and Discussion

Figure 1 illustrates the X-ray diffraction (XRD) patterns of the as-cast alloy plate and the consubstantial alloy powders synthesized by intermixing pure Zr, Cu, Ni, and Al powders through ball milling for 24 h. It can be seen that both XRD patterns consist of only one broad diffraction peak without any sharp Bragg peaks, indicating that the plate and alloy powders all are of amorphous structure. Figure 2a shows the schematic diagram of the outer morphology of the BMG plate after the amorphous alloy powders (AAPs) have been welded or melted onto the cleaned surface of the as-cast BMG plate, where 0# is the denotation token of the BMG matrix and 1#, 2#, and 3# refers to the location welded with 60 mA, 80 mA, and 100 mA beam currents, respectively. During the laser welding procedure, AAPs would melt and form semicircle mulches in the BMG surface. Eventually, the AAPs and the BMG would fuse into a whole. Figure 2b shows the schematic diagram of the outer morphology of the welded BMG plate after the semicircle mulches have been removed. Figure 2c exhibits the plate-like ZrCuNiAl BMG prepared via rapid solidification technology. In Figure 2d, one of the welds is shown as an example.

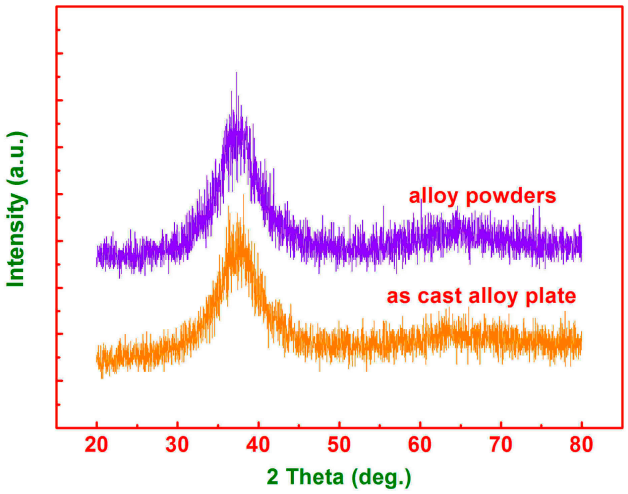

Figure 1. X-ray diffraction (XRD) patterns for the as-cast alloy and consubstantial alloy powders.

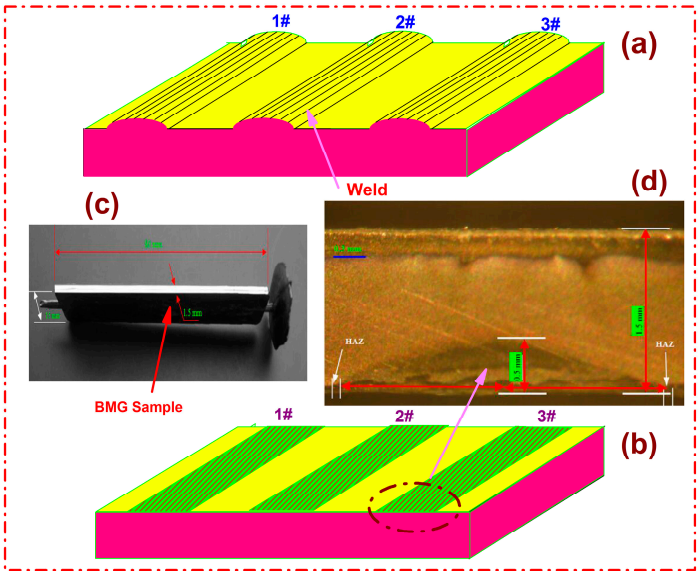

Figure 2. Schematic diagrams of the welded bulk metallic glass (BMG) plate (**a**) before and (**b**) after the semicircle mulches have been removed; (**c**) the as-cast plate-like BMG sample; and (**d**) a weld.

After laser welding procedures, all the removed semicircle mulches, corresponding to the welds denoted as 1#, 2#, and 3#, respectively, were further verified by XRD. The XRD patterns (not shown in the present paper) validate again the amorphous nature of the welds. Figure 3 exhibits the differential scanning calorimetry (DSC) curves measured at a heating rate of 20 K/min for 0#, 1#, 2#, and 3#, respectively. The glass transition temperatures (T_g), the onset temperatures of exothermic reaction (T_x), the crystallization exothermic peak (T_p), the super-cooled liquid regions $\Delta T_x = (T_x - T_g)$ of the matrix, and welds are summarized in Table 1 and shown in Figure 4. T_g, T_x, T_p, and ΔT_x of the amorphous matrix were measured to be 690.6, 758.9, 765.83, and 68.3 K, respectively. With the energy inputs, T_g is largely unchanged, while T_x and T_p both presented a certain change trend, i.e., their values first increased and then decreased. After laser welding, T_x was enhanced by 3.8 K for 1#, 6.3 K for 2#, and -2.6 K for 3#, respectively. Meanwhile, T_p was increased by 3.8 K for 1#, 6.2 K for 2#, and -2.5 K for 3#, respectively. ΔT_x was measured to be 71.9, 74.1, and 65.4 K for 1#, 2#, and 3#, respectively. ΔT_x of 1# increased by 3.6 K, while that of 2# increased more, reaching 5.8 K. With the further increase of energy, ΔT_x of 3# was 2.9 K less than that of 0#. Laser rapid melting and solidification processes have a certain effect on the thermodynamic parameters of the ZrCuNiAl BMG. The highest value of ΔT_x, 74.1 K, is obtained when the beam current is 80 mA, which is a relatively large value and indicates that the thermal stability against the crystallization of the weld of 2# has been enhanced and strengthened [23]. Figure 5 shows the crystallization volume fraction x as a function of temperature T under a heating rate of 20 K/min for the BMG and the three welds, respectively. All relation curves between x and T exhibit an S-like shape. With the increase of welding current, the crystallization rate of x vs. T descends gradually, indicating obvious kinetic effects in the crystallization events, i.e., the higher the welding current, the wider the temperature range for crystallization. Meanwhile, when the input current increases up to 100 mA, x/T rises and even exceeds that of the BMG matrix, which is very consistent with the DSC analysis.

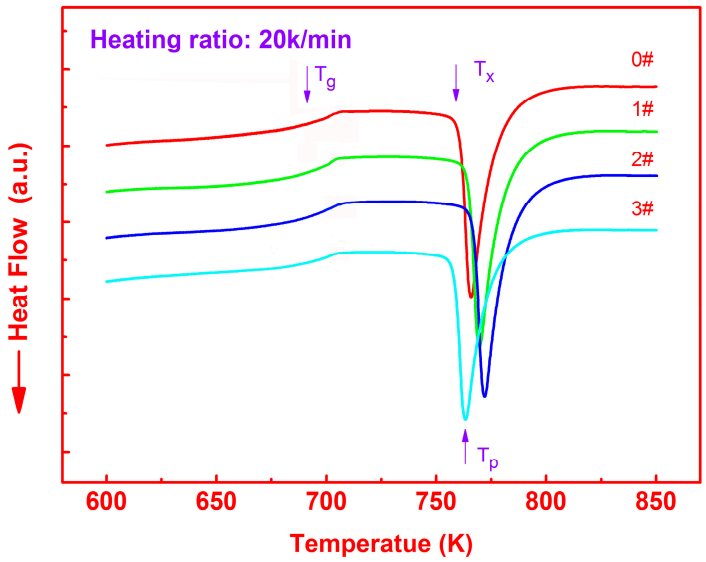

Figure 3. Differential scanning calorimetry (DSC) curves for the BMG matrix and welds processed with different currents.

Table 1. Characteristic parameters for thermodynamics of the BMG matrix and three welds.

BMG	T_g/K	T_x/K	T_p/K	ΔT_x/K
0#	690.6	758.9	765.8	68.3
1#	690.8	762.7	769.6	71.9
2#	691.1	765.2	772.0	74.1
3#	690.9	756.3	763.3	65.4

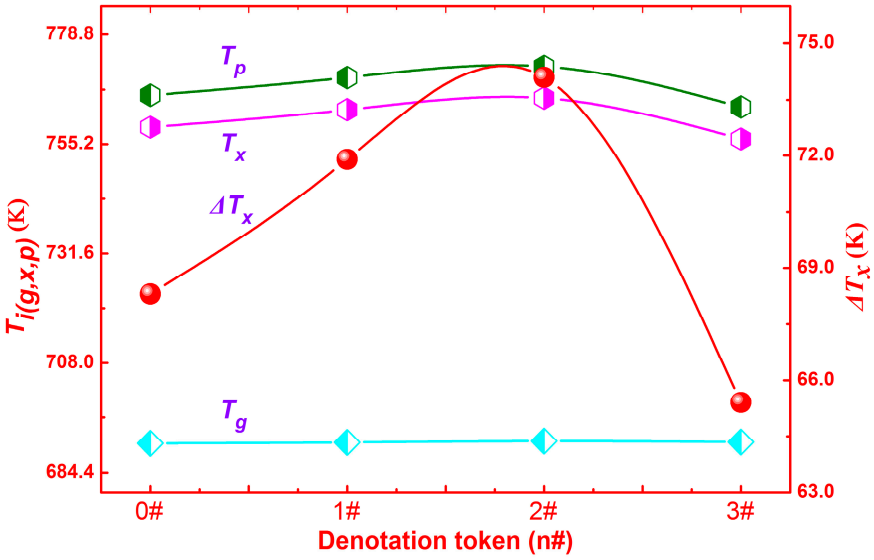

Figure 4. The variations of thermodynamic parameters for the BMG matrix and welds processed with different currents.

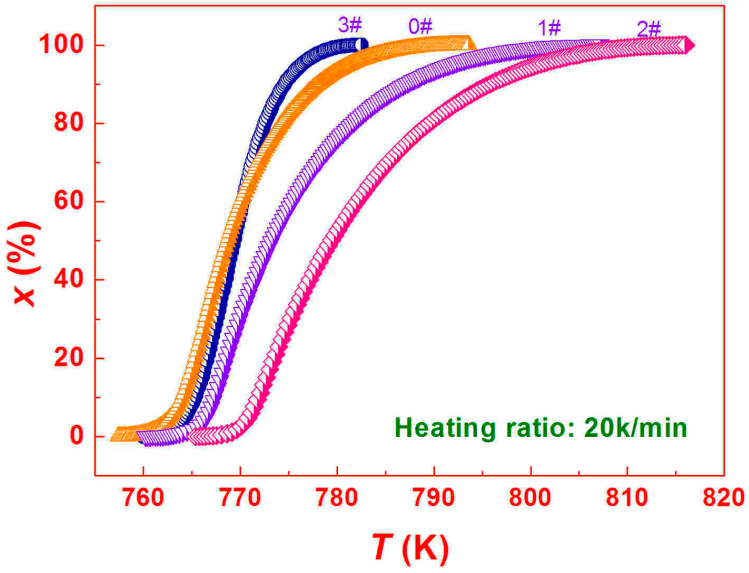

Figure 5. Crystallization volume fraction x vs. temperature T for the BMG matrix and welds processed with different currents.

Figure 6 presents $\Delta H_i/\Delta H_0$ for the welds processed with different currents, where ΔH_i and ΔH_0 refers to the released enthalpy through crystallization for the welds and the BMG matrix, respectively. The variation in the released enthalpy is the signal of increase or decrease of thermal enthalpy in a weld. If enthalpy in a weld increases, $\Delta H_i/\Delta H_0$ would be larger than 1, and vice versa. In Figure 6, along the oa straight line, $\Delta H_i/\Delta H_0$ increases gradually up to 16% for 1# and 23% for 2#, respectively. After oa and ab intersect, it varies along the ab straight line and eventually arrives to point b, i.e., $\Delta H_i/\Delta H_0$ lowers nearly 10%. In the selected current range in the present paper, variation of $\Delta H_i/\Delta H_0$ would be confined within the triangle oab. During the welding procedure, the energy inputs would melt local coating alloy powders and the BMG matrix to form a weld. Cooling down from a molten state to a solid state, the enthalpy level in the weld would change significantly. The increase in enthalpy could be attributed to the undersaturation of enthalpy produced during BMG fabrication, which offers a reserve capability for enthalpy when energy inputs are in progress. The 1# and 2# welds meet this situation,

while for 3#, the increased enthalpy has exceeded the reserve capability, and redundant energy acts as the driving force in atomic rearrangement. Once the atomic rearrangements take place, enthalpy begins to decline rapidly. New enthalpy change area due to reverse energy inputs and local atomic rearrangement structural relaxation would form in the left triangle area created by the oa line and the ob line reverse intersection. The high-resolution transmission electron microscopy (HRTEM) images of 1# and 2# are very similar to that of 0#. For a comparison, the bright field images (BFIs) and selected area diffraction patterns (SADs) of 0# and 3# are demonstrated, as shown in Figures 7 and 8, respectively. The TEM results show that there was no crystallization in 1#. Some crystalline phases could be observed in 3# even though crystalline phases could not be detected from the XRD pattern, indicating the occurrence of structural rearrangements during the welding procedure. Through measurement, the biggest dimensions of the precipitated crystallites are less than 6 nm, which can not be detected in the XRD pattern due to the sensitivity limits of XRD analysis methods. The TEM findings are very consistent with the results and analysis from Figures 3–5. As to 1# and 2#, the increased enthalpies produced by the energy inputs have not exceeded the reserve capability of enthalpy in the BMG matrix. The newly forming atomic packing states would store more enthalpies, resulting in higher thermodynamic parameters and thermal stabilities as well as lower crystallization rates. For 3#, the enthalpy increases over its saturation, and, subsequently, large-scale atomic rearrangements have been activated, leading to the formation of precipitated crystallites. The precipitated crystallites could serve as the crystal nucleuses [24], resulting in a higher crystallization rate and subsequently lower thermodynamic parameter and thermal stability.

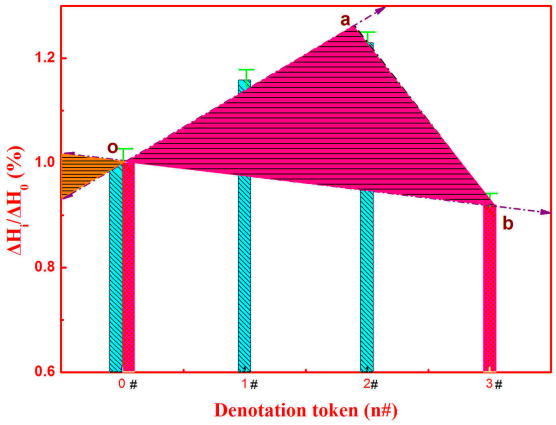

Figure 6. $\Delta H_i/\Delta H_0$ for the BMG matrix and welds processed with different currents.

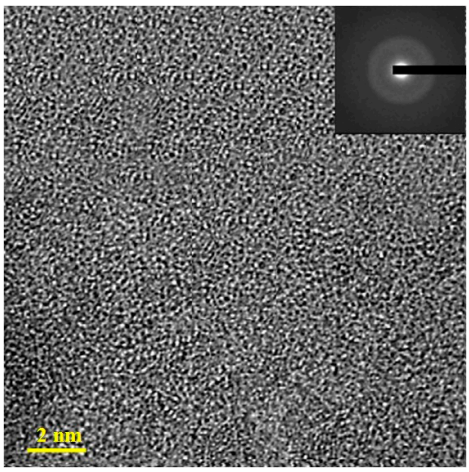

Figure 7. The bright field image and selected area diffraction pattern of the BMG matrix.

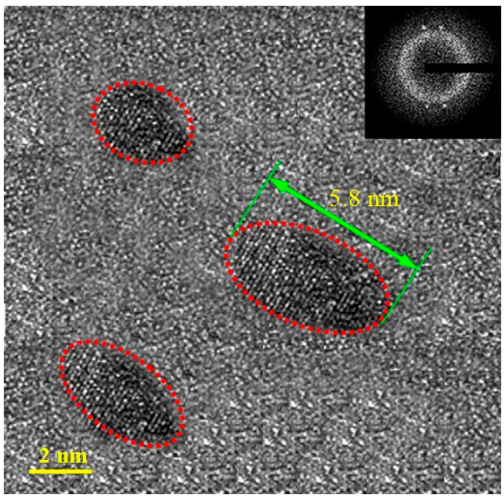

Figure 8. The bright field image and selected area diffraction pattern of the 3# weld.

Micro-hardness values are plotted for the BMG matrix and different welds as shown in Figure 9, where *R + 3 mm* refers to the micro-hardness values obtained from the measured spots 3 mm away from the right side, and *R or L + 5 mm* and *L + 3 mm* have similar implications. The mean micro-hardness in the BMG matrix is about 550 Hv. All datum groups exhibit similar trends, indicating the homogeneity for the mechanical property in the welds. When the current grows from 60 mA to 80 mA, the values in micro-hardness augment from about 2% to 5%, being attributed to the increased enthalpies in the welds and more mismatched extents in atom random stacking or packing [22]. When welding with a current of up to 100 mA, the micro-hardness in the weld rapidly increases by approximately 33% due to the formation of precipitated crystallites in the weld as illustrated in Figure 8. If the molecular dynamics were used to simulate the distribution of micro-hardness for each weld, the micro-hardness value in the weld as well as in both of its side areas could be plotted as shown in Figure 10. It can be found that, for all welding procedures, micro-hardness values in the HAZs would decrease. The maximum declines of micro-hardness in the HAZs could be calculated to be 3.8%, 4.6%, and 5.1% for 1#, 2#, and 3#, respectively. Then, the micro-hardness would increase gradually, and the maximum value would be observed in the center of each weld. The micro-hardness datum curve presents a basically symmetrical character. Compared with values from actual measurements, the micro-hardness in HAZs decreases by 2.2%, 2.9%, and 2.5% for 1#, 2#, and 3#, respectively, while that in the weld center increases by 1.9%, 3.1%, and 23.1%, respectively.

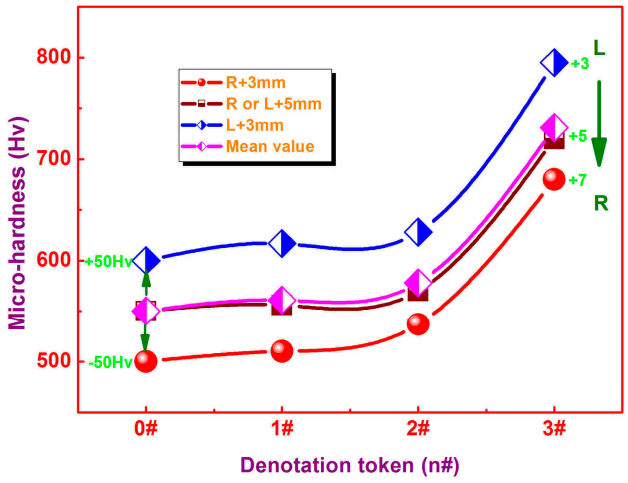

Figure 9. Micro-hardness at different locations for the BMG matrix and different welds.

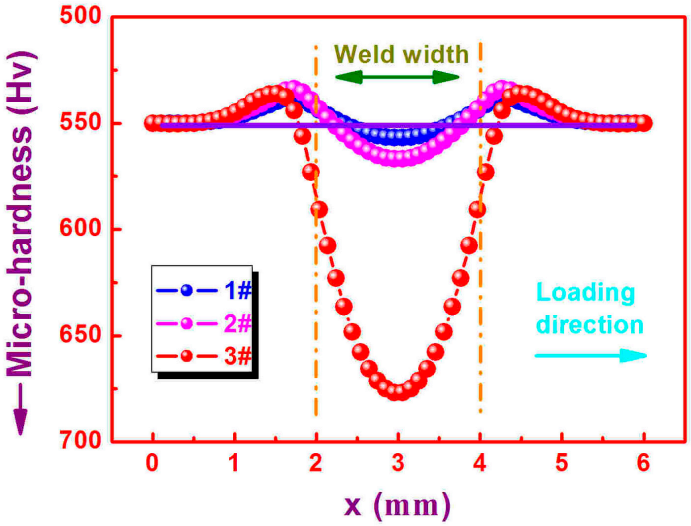

Figure 10. The simulated micro-hardness distributions along transverse direction in the welds and their both side areas.

4. Conclusions

In conclusion, a $Zr_{55}Cu_{30}Ni_5Al_{10}$ plate-like BMG was prepared using copper mold suction casting. Additionally, the consubstantial alloy powders were synthesized through ball milling. The alloy powders were welded or melted to the cleaned surface of the BMG with a laser beam acceleration voltage of 60 kV, a beam current range from 60 to 100 mA, a welding speed of 60 mm/s, as well as an impulse width of 3.0 ms. The effect of consubstantial composition welding on the microstructures and properties in BMG was investigated. Experimental results in this paper show that the consubstantial composition laser welding and different laser welding process parameters could affect the microstructures and properties of the Zr-based BMG. The molten and subsequently solidified metallic mixtures remain an amorphous structure. With the energy inputs, T_g is largely unchanged, while both T_x and T_p first increase and then decrease. When the beam current is 80 mA, the highest value of ΔT_x, 74.1 K, can be obtained. Appropriate laser welding parameters can enhance and strengthen the thermal stability against crystallization for BMGs. The enthalpy in the welds processed with different currents varies due to the combination of the micro-structural relaxation and nano-crystals precipitated during the energy inputs. The surface layers of the BMG can be significantly intensified after the laser welding treatments. However, the HAZs exhibit a slight degradation in mechanical properties with respect to the BMG matrix.

Acknowledgments: This work is supported by the National Natural Science Foundation of China (51201038), the Higher Specialized Research Foundation for Doctoral Program (20124420120009, 20124420110007), the National Natural Science Foundation of Guangdong (2015A030313488), the Public Welfare Research and Capacity Building Project of Guangdong (2015A010105028, 2016A010103033), the Collaborative Innovation and Environmental Platform Capacity Building Project of Guangdong (2015B090901005, 2016B090918088, 2016B090918081, 2016B090918052), and the Applied Science and Technology Research Project (2015B010127003), and the Guangzhou Science and Technology Project (201607010052).

Author Contributions: Pingjun Tao conceived and designed the experiments, wrote and edited the manuscript, and contributed to all activities. Qi Tu and Wenwu Zhang performed the XRD, DSC, and SEM experiments. Yuanzheng Yang helped to finish the experiments, to analyze the results, and to revise the manuscript.

Conflicts of Interest: The authors declare no conflict of interest.

References

1. Kuwabara, J.; Yasuda, T.; Takase, N.; Kanbara, T. Effects of the Terminal Structure, Purity, and Molecular Weight of an Amorphous Conjugated Polymer on Its Photovoltaic Characteristics. *ACS Appl. Mater. Interfaces* **2016**, *8*, 1752–1758. [CrossRef] [PubMed]

2. Prutsch, D.; Wilkening, M.; Hanzu, I. Long-Cycle-Life Na-Ion Anodes Based on Amorphous Titania Nanotubes-Interfaces and Diffusion. *ACS Appl. Mater. Interfaces* **2015**, *7*, 25757–25769. [CrossRef] [PubMed]
3. Wang, W.H.; Dong, C.; Shek, C.H. Bulk Metallic Glasses. *Mater. Sci. Eng. R* **2004**, *44*, 45–89. [CrossRef]
4. Gordon, L.M.; Cohen, M.J.; MacRenaris, K.W.; Pasteris, J.D.; Seda, T.; Joester, D. Amorphous Intergranular Phases Control the Properties of Rodent Tooth Enamel. *Science* **2015**, *347*, 746–750. [CrossRef] [PubMed]
5. Wang, J.; Wu, C.-Y.; Franke, G. Effectiveness of Amorphous Silica Encapsulation Technology on Welding Fume Particles and Its Impact on Mechanical Properties of Welds. *Mater. Des.* **2014**, *54*, 79–86. [CrossRef]
6. Fard, Z.H.; Islam, S.M.; Kanatzidis, M.G. Porous Amorphous Chalcogenides as Selective Adsorbents for Heavy Metals. *Chem. Mater.* **2015**, *27*, 6189–6192. [CrossRef]
7. Pauly, S.; Gorantla, S.; Wang, G.; Kuehn, U.; Eckert, J. Transformation-mediated Ductility in CuZr-based Bulk Metallic Glasses. *Nat. Mater.* **2010**, *9*, 473–477. [CrossRef] [PubMed]
8. Tao, P.J.; Yang, Y.Z.; Bai, X.J.; Mu, Z.X.; Li, G.Q.; Xie, Z.W.; Chen, X.C. Study on Implantation of Co Ions in ZrCuNiAl Bulk Metallic Glass. *Surf. Coat. Technol.* **2009**, *203*, 1656–1659. [CrossRef]
9. Duan, G.; Blauwe, K.D.; Lind, M.L.; Schramm, J.P.; Johnson, W.L. Compositional Dependence of Thermal, Elastic, and Mechanical Properties in Cu-Zr-Ag Bulk Metallic Glasses. *Scr. Mater.* **2008**, *58*, 159–162. [CrossRef]
10. Li, Y.; Guo, Q.; Kalb, J.A.; Thompson, C.V. Matching Glass-Forming Ability with the Density of the Amorphous Phase. *Science* **2008**, *322*, 1816–1819. [CrossRef] [PubMed]
11. Singer, J.P.; Gopinadhan, M.; Shao, Z.; Taylor, A.D.; Schroers, J.; Osuji, C.O. Nanoimprinting Sub-100 nm Features in a Photovoltaic Nanocomposite using Durable Bulk Metallic Glass Molds. *ACS Appl. Mater. Interfaces* **2015**, *7*, 3456–3461. [CrossRef] [PubMed]
12. Shahabi, H.S.; Scudino, S.; Kaban, I.; Stoica, M.; Rütt, U.; Kühn, U.; Eckert, J. Structural Aspects of Elasto-plastic Deformation of a Zr-based Bulk Metallic Glass under Uniaxial Compression. *Acta Mater.* **2015**, *95*, 30–36. [CrossRef]
13. Granata, D.; Fischer, E.; Loffler, J.F. Effectiveness of Hydrogen Microalloying in Bulk Metallic Glass Design. *Acta Mater.* **2015**, *99*, 415–421. [CrossRef]
14. Epp, V.; Ma, Q.L.; Hammer, E.M.; Tietz, F.; Wilkening, M. Very Fast Bulk Li Ion Diffusivity in Crystalline $Li_{1.5}Al_{0.5}Ti_{1.5}(PO_4)_3$ as Seen Using NMR Relaxometry. *Phys. Chem. Chem. Phys.* **2015**, *17*, 32115–32121. [CrossRef] [PubMed]
15. Ratzke, K.; Zollmer, V.; Bartsch, A.; Meyer, A.; Faupel, F. Diffusion in Bulk-metallic Glass-forming Pd-Cu-Ni-P alloys: From the Glass to the Equilibrium Melt. *J. Non-Cryst. Solids* **2007**, *353*, 3285–3289. [CrossRef]
16. Jin, K.; Loffler, J.F. Bulk metallic glass formation in Zr-Cu-Fe-Al alloys. *Appl. Phys. Lett.* **2005**. [CrossRef]
17. Inoue, A.; Zhang, T.; Nishiyama, N.; Ohba, K.; Masumoto, T. Preparation of 16 mm Diameter Rod of Amorphous $Zr_{65}Al_{7.5}Ni_{10}Cu_{17.5}$ Alloy. *Mater. Trans.* **1993**, *34*, 1234–1237. [CrossRef]
18. Tao, P.; Yang, Y. Effect of Aspect-ratio Alterations on Plastic-deformation-behavior of a Large-plastic Bulk Metallic Glass. *Mater. Des.* **2015**, *73*, 10–14. [CrossRef]
19. Wang, H.S.; Chiou, M.S.; Chen, H.G.; Jang, J.S.C. The effects of Initial Welding Temperature and Welding Parameters on the Crystallization Behaviors of Laser Spot Welded Zr-based Bulk Metallic Glass. *Mater. Chem. Phys.* **2011**, *129*, 547–552. [CrossRef]
20. Shin, H.S.; Park, J.S.; Jung, Y.C.; Ahn, J.H.; Yokoyama, Y.; Inoue, A. Similar and Dissimilar Friction Welding of Zr-Cu-Al Bulk Glassy Alloys. *J. Alloy. Compd.* **2009**, *483*, 182–185. [CrossRef]
21. Wang, D.; Xiao, B.L.; Ma, Z.Y.; Zhang, H.F. Friction Stir Welding of $Zr_{55}Cu_{30}Al_{10}Ni_5$ Bulk Metallic Glass to Al-Zn-Mg-Cu Alloy. *Scr. Mater.* **2009**, *60*, 112–115. [CrossRef]
22. Kim, J.; Kawamura, Y. Dissimilar Welding of $Zr_{41}Be_{23}Ti_{14}Cu_{12}Ni_{10}$ Bulk Metallic Glass and Stainless Steel. *Scr. Mater.* **2011**, *65*, 1033–1036. [CrossRef]
23. Cheung, T.L.; Shek, C.H. Thermal and mechanical properties of Cu-Zr-Al bulk metallic glasses. *J. Alloy. Compd.* **2007**, *434–435*, 71–74. [CrossRef]
24. Bian, Z.; Wang, R.J.; Wang, W.H. Carbon-nanotube-reinforced Zr-based Bulk Metallic Glass Composites and Their Properties. *Adv. Funct. Mater.* **2004**, *14*, 55–63. [CrossRef]